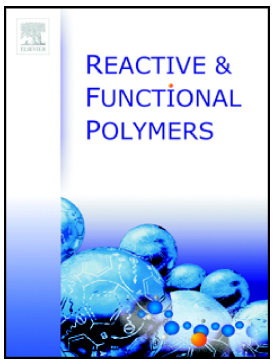

Chimeric poly(N-isopropylacrylamide)-b-poly(3,4-dihydroxy-L-phenylalanine) nanocarriers for temperature/pH dual-stimuli-responsive theranostic application

Rimesh Augustine, Dae-Kyoung Kim, Su Hyeon Jeon, Tae Wook Lee, Nagendra Kalva, Jae Ho Kim, Il Kim

PII: S1381-5148(20)30195-4

DOI: https://doi.org/10.1016/j.reactfunctpolym.2020.104595

Reference: REACT 104595

To appear in: *Reactive and Functional Polymers*

Received date: 12 February 2020

Revised date: 3 April 2020

Accepted date: 7 April 2020

Please cite this article as: R. Augustine, D.-K. Kim, S.H. Jeon, et al., Chimeric poly(N-isopropylacrylamide)-b-poly(3,4-dihydroxy-L-phenylalanine) nanocarriers for temperature/pH dual-stimuli-responsive theranostic application, *Reactive and Functional Polymers* (2019), https://doi.org/10.1016/j.reactfunctpolym.2020.104595

Chimeric poly(*N*-isopropylacrylamide)-*b*-poly(3,4-dihydroxy-*L*-phenylalanine) nanocarriers for temperature/pH dual-stimuli-responsive theranostic application

Rimesh Augustine[a], Dae-Kyoung Kim[b], Su Hyeon Jeon[a], Tae Wook Lee[b], Nagendra Kalva[a], Jae Ho Kim[b,*], Il Kim[a,*]

[a]BK21 PLUS Center for Advanced Chemical Technology, Department of Polymer Science and Engineering, Pusan National University, Busan 609-735, Republic of Korea.

[b]Department of Physiology, School of Medicine, Pusan National University, Yangsan 626-870, Gyeongsangnam-do, Republic of Korea.

*Corresponding Author:

E-mail: ilkim@pusan.ac.kr (I. Kim); jhkimsrt@pusan.ac.kr (J.H. Kim)

Abstract

A series of poly(*N*-isopropylacrylamide)$_{60}$-*block*-poly(3,4-dihydroxy-*L*-phenylalanine)$_n$ (p(NIPAM)$_{60}$-*b*-p(DOPA)$_n$) (n = 30, 50, 75, 100) copolymers have been prepared by combining reversible addition fragmentation chain transfer polymerization with ring opening polymerization of *N*-carboxyanhydride α-amino acid using *N*-heterocyclic carbene as an organocatalyst. The copolymers form spherical nanoparticles with an average diameter of ~100 nm by self-assembly. Doxorubicin (Dox) is encapsulated in the spherical nanocarriers with a drug loading efficiency of 44.2%. The iron(III) ions are coordinated to the copolymer matrix via catechol moieties in p(DOPA) units, resulting in temperature/pH dual-stimuli-responsive nanocarriers. The microstructures and Dox loading procedure can be predicted using a dissipative particle dynamics simulation. Cellular uptake and theranostic anticancer activity studies reveal that the nanocarriers release encapsulated Dox preferentially in cancer cells in response to morphological changes induced by variations in temperature and pH. Both cell internalization and cytotoxicity in A2780 ovarian cancer cells and *in vivo* biodistribution studies demonstrate that the Dox-loaded nanocarriers fabricated by p(NIPAM)-*b*-p(DOPA) copolymers can be a promising candidate for cancer therapy.

Keywords: block copolymers; drug delivery; poly(*N*-isopropylacrylamide); poly(3,4-dihydroxy-*L*-phenylalanine); polypeptides; responsive polymers

1. Introduction

During the past few decades, great advances have been made in the cancer treatments. The current methods for treatment of tumors are mainly surgery, radiotherapy, chemotherapy and immunotherapy. Chemotherapy is one of the most widely studied therapeutic methods for various types of cancers. However, the drugs used in chemotherapy confront with non-targeted distribution, leading to the simultaneous impairment of normal cells while destroying the cancer cells [1]. This has fuelled an urgent demand for biocompatible carrier molecules with site-specific release of drugs in cancer cells. Polypeptide nanocarriers are increasingly used in clinical application and have been proven useful for drug delivery due to their biocompatibility, biodegradability, stimuli-responsive nature and precise targetability [2–6]. Diblock polypeptides have earned distinction in this category due to their improved therapeutic efficiency in terms of high drug loading capacity, solubility, prolonged circulation, drug releasing ability in response to the physiological conditions of cancerous environments, and the tendency to form interesting nanoscale morphologies in aqueous solution [7–10].

The stimuli-responsive polymer nanocarriers have considerable prospects for the effective drug delivery to a targeted site. Recently, sytems responding to two or three or more signals such as pH, temperature, redox reactions, magnetic fields, diols, guest molecules, and enzymes have been demonstrated to exhibit enhanced theranostic efficacy [11–16]. Specifically, pH- and temperature-responsive systems have been widely investigated to take advantages of the different environments of cancer cells from normal cells with respect to pH and temperature [17,18]. Owing to the fast proliferation of cancer cells, the endogeneous temperature in cancer cells is higher than the normal cells [19]. Moreover, the high glycolysis rate at aeraobic and anaeraobic conditions in tumor increases the acidity in tumor extracellular environment [20]. The pH even drops to more acidic in endosomes (pH 5.5) and in lysosomes (4.5–5.0) [21,22]. This pH gradient between normal and cancer cells offers tremendous opportunity to develop diverse pH-responsive drug carrier platforms to increase the drug concentration in tumor and thereby achieving high therapeutic index. Tremendous polymeric nanocarriers have been developed by

introducing pH-responsive monomers and acid-labile linkages. The acid-labile linkages such as acetal, hydrazone, schiff base, ortho ester and β-thiopropionate were extensively investigated for the fast drug release in the tumor cells.

3,4-Dihydroxy-*L*-phenylalanine (*L*-DOPA), a main amino acid comprising the protein of sea mussels, shows adhesive, water resistant, and fast-curing properties. The pendant catechol group in *L*-DOPA is the source of the strong adhesive property of the *L*-DOPA-derived protein due to a strong affinity to bind metal ions [23–25]. The stable bis-complex formed between catechol moiety in *L*-DOPA and Fe^{3+} at pH 7.4 dissociates to mono-complex at pH 5.0, recommending the polymer systems bearing *L*-DOPA to use as auspicious pH-responsive drug carrier. In the present work, we have fabricated temperature/pH dual-stimuli-responsive spherical nanocarriers using a series of poly(*N*-isopropylacrylamide)$_{60}$-*block*-poly(*L*-dihydroxyphenylalanine)$_n$ (p(NIPAM)$_{60}$-*b*-p(DOPA)$_n$) (n = 30, 50, 75, 100) copolymers, where p(NIPAM) block and Fe^{3+}-coordinated p(*L*-DOPA) block show temperature and pH responses, respectively (Scheme 1). The diblock copolymers were synthesized using the combination of reversible addition fragmentation chain transfer (RAFT) polymerization and ring-opening polymerization (ROP) of *N*-carboxyanhydride (NCA), where p(NIPAM)-NH_2 used as a macroinitiator for the ROP of di-*O,O,*-acetyl-*L*-DOPA-*N*-carboxyanhydride ((AC$_2$)-DOPA-NCA) in the presence of 1,3-dicyclohexylimidazolium hydrogen carbonate (ICy·HCO_3) as an organocatalyst,. The diblock copolymers were self-assembles into nanocarriers with a suitable size for theranostic application. The cytotoxicity of the nanocarriers was tested with 293FT normal kidney cells and A2780 ovarian cancer cells. The doxorubicin (Dox)-loaded polymer nanocarriers were also utilized to investigate the temperature/pH dual-stimuli-responsive *in vitro* Dox release and the intracellular drug internalization using the A2780 ovarian cancer cells. The newly designed theranostic nanocarriers released Dox molecules preferably in a cancerous environment by responding to the pH and temperature of tumor cells.

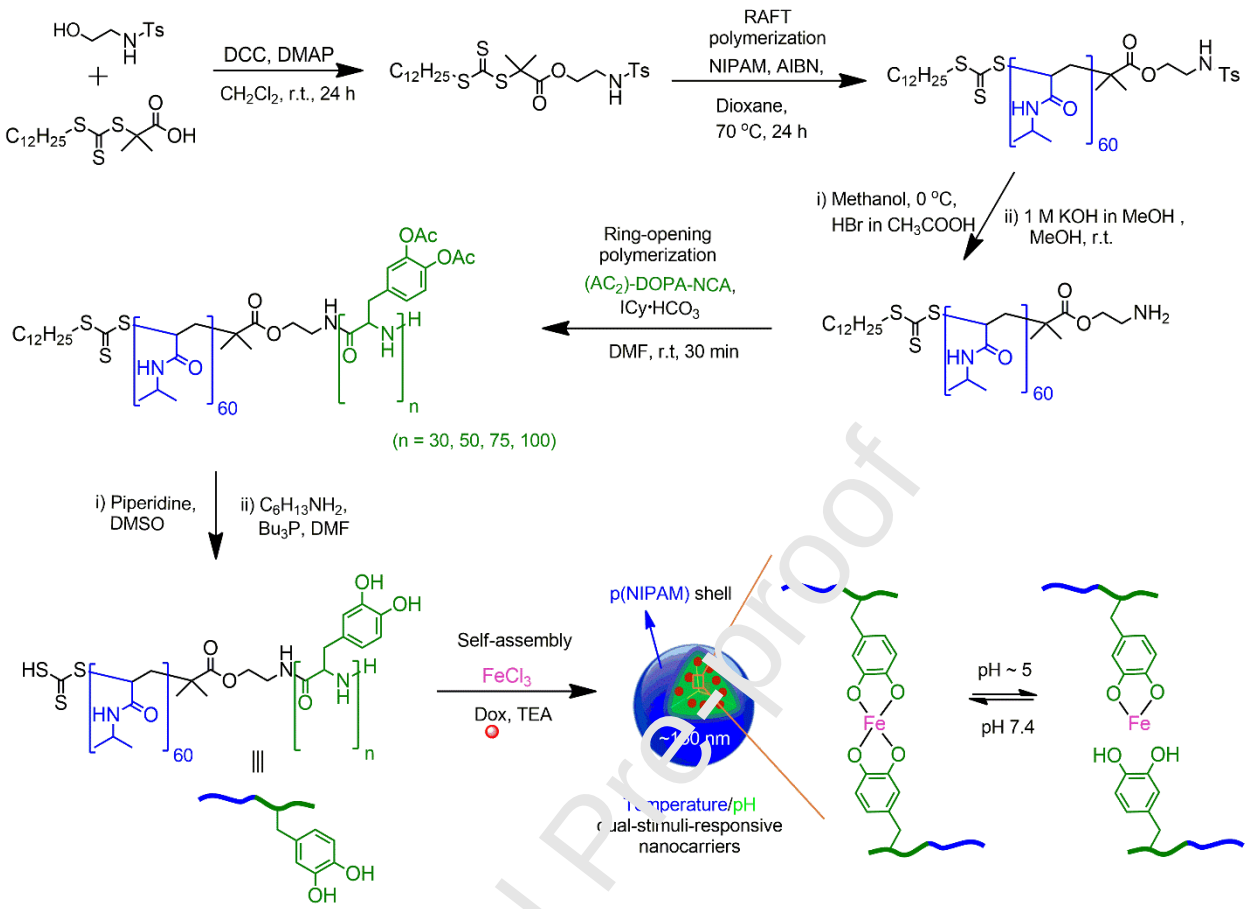

Scheme 1. Synthesis of p(NIPAM)$_{60}$-*b*-p(DOPA)$_n$ (n = 30, 50, 75, 100) diblock copolymers by combining a RAFT polymerization of NIPAM with an organocatalyzed ROP of (AC_2)-DOPA-NCA and the fabrication of Fe^{3+} conjugated nanocarriers with Dox encapsualtion.

2. Experimental

2.1. Materials

Triethylamine (TEA, 99.5%), 2-amino ethanol (97%), paratoluene sulfonyl chloride (99%), 2-(dodecylthiocarbonothioylthio)-2-methylpropanoic acid (chain transfer agent-1, CTA-1), 4-dimethylamino pyridine (DMAP, 99%), 2,2'-azobis(2-methylpropionitrile) (AIBN, 98%), *N*,*N*'-dicyclohexylcarbodiimide (DCC, 99.0%), 1,3-dicyclohexylimidazolium chloride (ICy·Cl) and acetic anhydride were all purchased from Sigma-Aldrich and used without further purifications. *N*-Isopropylacrylamide (NIPAM, 97%) was purchased from Acros Organics and recrystallized from hexane. Doxorubicin hydrochloride (≥99%) was purchased from Lancrix Chemicals (Shanghai, China). 3-(3,4-Dihydroxyphenyl)-L-alanine (*L*-DOPA) and triphosgene (>98.0%)

were purchased from TCI (Tokyo, Japan). Piperidine (99%) was purchased from Alfa Aesar. Solvents such as *N,N*-dimethylformamide (DMF) and *N,N*-dimethyl acetamide (DMAc) were distilled over sodium, whereas acetone and chloroform were distilled over calcium hydride. Other reagent grade chemicals were purchased from Sigma-Aldrich or TCI and used without further purification.

2.2. Synthesis of p(NIPAM)-NH_2

p(NIPAM)-NH_2 with the desired molecular weight (MW) was synthesized according to the literature [26]. Detailed procedures of CTA-2 and p(NIPAM)-NH_2 synthesis are given in the Supporting Information.

2.3. Synthesis of p(NIPAM)-b-p(L-DOPA)

2.3.1. Synthesis of (AC_2)-DOPA-NCA

(AC_2)-DOPA NCA was prepared in two steps as described in the literature [27]. Detailed procedure of (AC_2)-DOPA-NCA is given in the Supporting Information.

2.3.2. Synthesis of p(NIPAM)-b-p(L-DOPA) copolymers

A series of p(NIPAM)-*b*-p(*L*-DOPA) copolymers were synthesized by the ROP of (AC_2)-DOPA-NCA using $p(NIPAM)_{60}$−NH_2 as a macroinitiator and ICy·HCO_3 as the organocatalyst. $p(NIPAM)_{60}$−NH_2 (0.91 g, 0.16 mmol) was dissolved in dry DMF (32 mL) in a 100 mL Schlenk round-bottom flask under nitrogen. A solution of (AC_2)-DOPA-NCA (0.79 g, 4.8 mmol) in DMF (2 mL) was added to the Schlenk round-bottom flask containing $p(NIPAM)_{60}$−NH_2. The mixture was stirred for 5 min and the ICy·HCO_3 catalyst (3 mg) directly synthesized from ICy·Cl was added; the reaction mixture was stirred under nitrogen at 30 °C for 30 min [28]. $p(NIPAM)_{60}$-p((AC_2)-DOPA) was obtained by repeated precipitation from diethyl ether. The resulting block copolymer was subjected to deprotection to remove the AC protecting groups. $p(NIPAM)_{60}$-p((AC_2)-DOPA) was dissolved in DMSO and bubbled with nitrogen for 5 min, followed by addition of piperidine (0.1 mL); the reaction mixture was stirred for 15 min at room temperature. The product was isolated by repeated precipitation from diethyl ether. This precipitate was then dissolved in 0.1 N HCl and dialyzed against aqueous HCl (pH 4.5). The membrane used for dialysis had a MW cut-off of 1,000. Dialysis followed by lyophilization yielded the deprotected

polymer (yield: 78%). ^{1}H NMR (400 MHz, DMSO): δ (ppm) = 1.02 (s, 6H), 1.52 (br,CH_2), 2.70 (t, 1H SCH), 2.75 (t, 2H CH2-C_6H_5), 3.94 (br, CH), 4.3 (m, 1H), 6.35−6.65 (m, 3H), 8.54 (s, OH).^{13}C NMR (100 MHz, DMSO) δ (ppm) = 21, 37.5, 49.9, 54.6, 115.6, 117.2, 120.4, 129.1, 144, 145.2, 169.1, 171.5. For the removal of the thiocarbonyl moiety by aminolysis p(NIPAM)$_{60}$-*b*-p(DOPA) was dissolved in DMF and stirred for 2 h under nitrogen at room temperature in the presence of *n*-hexylamine and tributylphosphine [29]. The thiol-terminated product was then obtained by repeated precipitation in cold diethyl ether, followed by drying under reduced pressure. The theoretical value of *L*-DOPA repeat unit of this copolymer was 30 and other copolymers having 50, 75 and 100 repeat units of *L*-DOPA were synthesized in a similar procedure by controlling [p(NIPAM)$_{60}$−NH_2]/[(AC_2)-DOPA-NCA] ratio.

2.4. Preparation of Dox-loaded polymer nanocarriers with catechol-Fe^{3+} complex

p(NIPAM)$_{60}$-*b*-p(DOPA)$_n$ (*n* = 30, 50, 75, 100) copolymers (30 mg) were dissolved in dimethylacetamide (21 mL) and stirred for 30 min. The nanocarriers were obtained by dropwise addition of deionized water (9 mL), followed by dialysis against deionized water for 48 h and subsequent lyophilization. The Dox-loaded p(NIPAM)$_{60}$-*b*-p(DOPA)$_{100}$ nanocarriers with catechol-Fe^{3+} complex were prepared by dissolving p(NIPAM)$_{60}$-*b*-p(DOPA)$_{100}$ copolymer (30 mg) in dimethylacetamide (21 mL) and stirred for 30 min. Later transferred to a 50 mL sample bottle containing Dox (15 mg) and TEA (90 µL) and stirred for 30 min. An aqueous solution of $FeCl_3$ (40 mM) is then added with feed ratio of [DOPA]/[Fe^{3+}] = 2/1 at pH 7.0 and stirred for 3 h. The nanocarriers were obtained by dropwise addition of deionized water (9 mL), followed by dialysis against deionized water for 48 h to remove the unloaded Dox and unreacted metallic ion and subsequent lyophilization to yield the Dox-loaded nanocarriers with catechol-Fe^{3+} complex derived cross-linking.

2.5. Determination of drug loading content (DLC), efficiency (DLE) and in vitro drug release

The drug-loaded nanocarriers were dissolved in DMSO (1 mL) and the solution was analyzed using UV-Vis spectroscopy. The characteristic absorption of Dox at 485 nm was compared with the of standard drug solutions of varying concentrations in DMSO. The percentage DLC and DLE were calculated using the following equations:

$$DLC\ (\%) = \frac{\text{weight of Dox in the nanocarriers}}{\text{weight of Dox loaded nanocarriers}} \times 100 \quad (1)$$

$$DLE\ (\%) = \frac{\text{weight of Dox in the nanocarriers}}{\text{weight of Dox for the preparation of drug loaded nanocarriers}} \times 100 \quad (2)$$

In vitro drug release studies were conducted by suspending the Dox-loaded nanocarriers in deionized water and placing them against a dialysis membrane that was subsequently placed in the required pH buffer and kept in a shaking bath. The amount of Dox released was measured by UV-Vis spectroscopy. The concentration of the released drug was determined by comparison with the standard curves for Dox in different pH buffers.

2.6. Characterizations

The proton nuclear magnetic resonance [^{1}H NMR, 400 MHz] and ^{13}C NMR [100 MHz] spectra were recorded using a Varian INOVA 400 NMR spectrometer. The chemical shifts are presented as parts per million (ppm) relative to the residual solvent peaks of the internal standard. The temperature-dependent ^{1}H NMR measurements were performed after the sample tube was allowed to equilibrate for approximately 10 min at each preset temperature. The singlet, doublet, triplet, multiplet, and broad multiplicity peaks in the ^{1}HNMR spectra are abbreviated as s, d, t, m, and br, respectively. Column chromatography was performed using a Combi-Flash Companion purification system (Teledyne ISCO) using 300−400 meshsilica gel. Fourier transform infrared (FTIR) spectra were recorded using a Shimadzu IR Prestige 21 spectrometer. The spectra were acquired using potassium bromide discs in the range of 4000–600 cm^{-1}. UV−Vis turbidimetry experiments were carried out for LCST determination on a Shimadzu UV-1650 PC, equipped with a temperature controller. Dynamic light scattering (DLS) measurements were performed using a Nano ZS90 zeta potential analyzer (Malvern Instruments, UK) with a He-Ne laser (633 nm), 90^0 collecting optics, and a thermoelectric Peltier temperature controller. The block copolymer solutions (2 mg mL^{-1}) were filtered through a 0.5-lM filter prior to use. The MW and polydispersity index ($Đ$) of the polymers were measured on a Waters GPC system, which was equipped with a Waters 1515 HPLC solvent pump, a Waters 2414 refractive index detector, and three Waters Styragel High Resolution columns (HR4, HR2, HR1; effective molecular weight range: 5000−500000, 500−20000, and 100−5000 g mol^{-1}, respectively) at 40 °C using HPLC grade DMF containing 0.1 N LiBr as the eluent at a flow rate of 1.0 mL min^{-1}. Monodisperse polystyrene was used to generate the calibration curve. The particle morphology was analyzed using transmission electron microscopy (TEM) with a JEOL-1299EX electron microscope at an accelerating voltage of 80 keV. The TEM samples were prepared in grids with formvar film and

treated with oxygen plasma (from a Harrick plasma cleaner/sterilizer) for 15 s to render the surface hydrophilic. The TEM grid was then floated on top of the bead with the hydrophilic surface in contact with the solution. The aqueous solution was blotted away with a strip of filter paper, and the samples were dried overnight at room temperature.

2.7. Cell culture

Ovarian cancer cells (A2780) and normal kidney cells (293FT) were cultured in Dulbecco's modified eagle medium (DMEM) supplemented with 10% fetal bovine serum (FBS) and penicillin/streptomycin and maintained at 37 °C under 5% CO_2 atmosphere.

2.8. Cytotoxicity assay

The proliferation was determined using a colorimetric 3-(4,5-dimethylthiazol-2-yl)-2,5-diphenyltetrazolium bromide (MTT) assay. To evaluate the cell proliferation, A2780 and 293FT cells were seeded into a 96-well culture plate at a density of 2×10^4 cells per well in serum-free DMEM medium. All cells were treated with polymer nanocarriers, and the analyses were performed in triplicate. After culturing the cells under the experimental conditions, the cells were washed twice with hank's balanced salt solution (HBSS) and incubated with 100 µL of MTT solution (0.5mg mL^{-1}) for 3 h at 37 °C. After incubation, the MTT solution was removed and the cells were treated with dimethylsulfoxide (DMSO; 100 µL/well), and the cell cytotoxicity was measured from the absorbance of the solution at 570 nm using a micro-plate spectrophotometer (TECAN) after dilution to the linear range. The percentage cell survival was expressed relative to an untreated control.

For flow cytometric analysis, the polymer nanocarrier-treated A2780 cells were incubated overnight. After washing with HBSS, the cells were harvested and analyzed using a flow cytometer (FACScan). The Dox fluorescence intensity was measured at an excitation wavelength of 488 nm and an emission wavelength of 522 nm.

2.9. In vivo bio-distribution

Bio-distribution studies of the Dox-encapsulated nanocarriers in different organs were carried out using tumor-bearing mice. Animal experiments were performed using protocols approved by the Pusan National University Institutional Animal Use and Care Committee. Tumor-bearing nude mice (male, age 6–9 weeks, weighing 22–24 g) were used for determining

the dynamics and bio-distribution of the Dox-loaded p(NIPAM)$_{60}$-*b*-p(*L*-DOPA)$_n$ nanocarriers for tumor imaging. Initially, tumor-bearing nude mice were prepared by injecting a suspension of 1×10^6 A2780 cells/mouse in PBS (pH 7.4, 200 μL) into the subcutaneous dorsa of athymic nude mice.

After the tumor volume reached approximately 5 mm^3 (about 15 days after inoculation), the Dox-loaded p(NIPAM)$_{60}$-*b*-p(DOPA)$_n$ nanocarriers were injected into the vein of the mouse and monitored for 72 h. The fluorescence images of the mice before treatment were acquired and set as the background. All images from the abdomen and the back were automatically acquired at 72 h after the injections and displayed with the same fluorescence intensity scale after background subtraction at 635 nm using the Maestro 2 *in vivo* imaging system (Cambridge Research and Instruments, Inc., Woburn, MA, USA). Before starting the experiments, the mice were anesthetized with an intraperitoneal injection of 400 mg kg^{-1} 2,2,2-tribromoethanol (Avertin; Sigma-Aldrich, St. Louis, MO). To confirm the bio-distribution of the Dox-loaded p(NIPAM)$_{60}$-*b*-p(DOPA)$_{100}$ nanocarriers in different organs, the mice were sacrificed 72 h after injection. Various organs were harvested, rinsed in saline, and imaged for fluorescence. Data are expressed as mean ± SD (n = 3).

3. Results and discussion

3.1. Synthesis of p(NIPAM)$_{60}$-b-p(L-DOPA)$_n$ and their thermo-responsive phase transition behavior

Synthesis of a series of p(NIPAM)$_{60}$-*b*-p(*L*-DOPA)$_n$ copolymers is summarized in Scheme 1. RAFT polymerization has been extensively used in preparing stimuli-responsive diblock and triblock polymers with low *Đ* value, uniform chemical composition and end-group reliability [30]. In this study, a trithiocarbonate CTA was modified by coupling with ethanolamine, where the amine group was protected with tosyl group. The tosyl protected RAFT agent was used in the polymerization of NIPAM to obtain p(NIPAM)$_{60}$ with narrow polydispersity. The tosyl groups were deprotected by acid hydrolysis to generate p(NIPAM)$_{60}$–NH_2, which can be used as a macroinitiator for the fast ROP of amino acid NCAs in the presence of ICy·HCO_3 organocatalyst [31]. The number average molecular weight (M_n) of p(NIPAM)–NH_2 was estimated to be 7400 (~60 repeating monomer units) using end-group analysis.

The ICy·HCO_3 catalyst yielded targeted MW of p[(AC_2)-DOPA-NCA] within 30 min by the ROP of (AC_2)-DOPA-NCA using p(NIPAM)$_{60}$–NH_2 as a macroinitiator. A series of block copolymers, p(NIPAM)$_{60}$-*b*-p[($AC)_2$-DOPA-NCA]$_n$ (*n* = 30, 50, 75, 100), were obtained simply by controlling [p(NIPAM)$_{60}$–NH_2]/ [(AC_2)-DOPA-NCA] ratio. The acetyl groups were deprotected to obtain p(NIPAM)$_{60}$-*b*-p(*L*-DOPA)$_n$ and then the thiocarbonylthio end-groups were removed by aminolysis. All compounds were characterized by NMR spectroscopy (see Figures S1−S6; Supporting Information). The block copolymers were also characterized by GPC and FT-IR spectroscopy (Figures S6 and S7). Table 1 summarizes the results of polymerization. The estimated block length of *L*-DOPA fits well with theoretical one with low *Đ* values. It is worth noting that the targeted block size of (AC_2)-DOPA-NCA can be achieved within 30 min in a living manner, much faster than conventional methods [28].

The temperature response of p(NIPAM)$_{60}$-*b*-p(*L*-DOPA)$_{50}$ was investigated by ^{1}H NMR spectroscopy using D_2O solvent in a range of 25–50 °C (Figure S8; Supporting Information). The spectra reveal that the proton signals assigned to NIPAM units are disappeared around the lower critical solution temperature (LCST) of p(NIPAM) due to conformational changes to the collapsed globule state caused by increased intramolecular hydrogen bonding between the C=O and –N(H)– groups and the accompanied increase of hydrophobicity [32]. The intensity of corresponding proton signals are gradually decreased at ~35 °C, and almost vanished above 45 °C, whereas the proton signals corresponding to DOPA are remained unaffected over the entire temperature range. This temperature responsive behavior of p(NIPAM) blocks can also be estimated by using UV-Vis spectrometry, since the turbidity is induced according to changes of solution temperature of the block copolymer in water. The transmittance variation plots according to temperature of p(NIPAM)$_{60}$-*b*-p(DOPA)$_{50}$ sample (Figure S9) clearly show that the LCST is observed around body temperature.

Table 1. Ring Opening Polymerization Results of (AC_2)-DOPA-NCA Initiated by p(NIPAM)-NH_2 Macroinitiator for the Synthesis of p(NIPAM)$_{60}$-*b*-p(DOPA)$_n$ (*n* = 30, 50, 75, 100)[a]

Sample	Theoretical composition	NCA[b] (mmol)	Yield (%)	M_n[c] (g/mol) Theo.[d]	M_n[c] (g/mol) NMR	M_n[c] (g/mol) GPC	NMR Composition	*Đ*

1	p(NIPAM)$_{60}$-*b*-p(DOPA)$_{30}$	4.8	69	12,300	12,100	16,100	p(NIPAM)$_{60}$-*b*-p(DOPA)$_{28}$	1.18
2	p(NIPAM)$_{60}$-*b*-p(DOPA)$_{50}$	8.0	65	15,900	15,800	21,800	p(NIPAM)$_{60}$-*b*-p(DOPA)$_{49}$	1.21
3	p(NIPAM)$_{60}$-*b*-p(DOPA)$_{75}$	12.0	68	20,500	20,000	25,200	p(NIPAM)$_{60}$-*b*-p(DOPA)$_{72}$	1.25
4	p(NIPAM)$_{60}$-*b*-p(DOPA)$_{100}$	16.0	70	25,100	24,600	30,500	p(NIPAM)$_{60}$-*b*-p(DOPA)$_{98}$	1.29

[a]Polymerization conditions: p(NIPAM)-NH_2= 0.91 g (0.16 mmol), 1,3-dicyclohexylimidazolium hydrogen carbonate (ICy·HCO_3) catalyst = 3 mg, DMF = 2 mL, temperature = 30 °C, time = 0.5 h.
[b]Amount of (AC_2)-DOPA-NCA monomer added to p(NIPAM)$_{60}$–NH_2 initiator.
[c]Number average molecular weight measured after deprotecting acetyl groups.
[d]M_n (theoretical) = {([(AC_2)-DOPA-NCA]$_0$/[p(NIPAM)$_{60}$-NH_2]$_0$) × (MW of repeating unit after deprotecting acetyl group) + (MW of initiator)}.

3.2. Fabrication of p(NIPAM)$_{60}$-b-p(L-DOPA)$_n$ nanocarriers and DPD simulations

To fabricate nanocarriers by self-assembly, 30 mg of block copolymer was dissolved in DMAc (21 mL) and deionized water (9 mL) was slowly added to the polymer solution. This solution was then dialyzed against deionized water to remove the organic solvent at 25 °C. Uniform and monodisperse spherical nanocarriers were obtained by self-assembly of all the p(NIPAM)$_{60}$-*b*-p(*L*-DOPA)$_n$ copolymers. The DLS analysis of aqueous solutions of copolymers shows that the average size of the resultant nanocarriers is in the range of 80–100 nm (Figure S10). The block length of p(*L*-DOPA) has a negligible effect on the nanocarrier size. According to TEM images of the nanocarriers (Figure S10), the nanocarriers have spherical morphologies and particle sizes are well agreeing with the DLS size distribution as shown in the insets. The p(NIPAM)$_{60}$-*b*-p(*L*-DOPA)$_{100}$ sample was chosen for further study including *in vivo* tests, since the nanocarriers fabricated by p(NIPAM)$_{60}$-*b*-p(*L*-DOPA)$_{100}$ sample show relatively uniform spherical morphology [Figure 1(a)] and have an average hydrodynamic size ~100 nm, which is sutable to achieve an enhanced permeability and retention (EPR) effect .

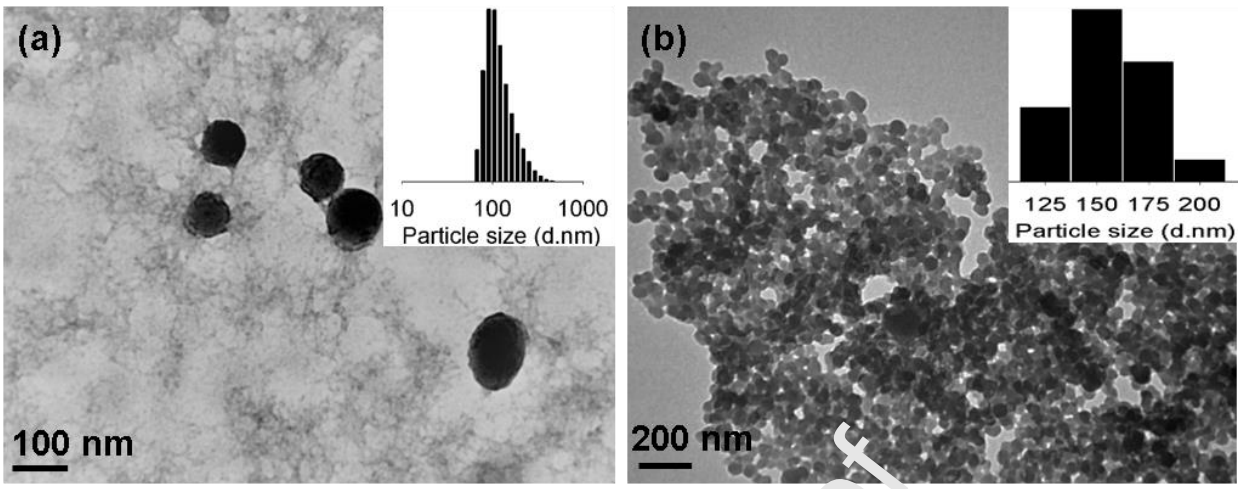

Figure 1. TEM images of nanocarriers fabricated by the self-assembly of (a) p(NIPAM)$_{60}$-*b*-p(DOPA)$_{100}$ and (b) p(NIPAM)$_{60}$-*b*-p(DOPA)$_{100}$ together with Dox and Fe^{3+} ions. Insets are the corresponding particle size distributions obtained using DLS

As a trial to understand the formation of nanocarriers and Dox loading/release mechanism of p(NIPAM)$_{60}$-*b*-p(*L*-DOPA)$_n$ copolymers the dissipative particle dynamics (DPD) simulations originally proposed by Hoogerbrugge and Koelmanin in 1992 and revised by Espa˜nol and Warren in 1995 were performed, since the results can provide a mesoscopic insight into the macroscale experimental system [33,34]. The combination with the bead-and-spring model makes it very appropriate for simulations on structure and dynamics of soft matter, where the time evolution of the interacting particles is governed by Newton's equation of motion [34,35]. The underlying principle of DPD theory is well-described in previous reports [35,36]. The DPD interaction parameters are obtained in two steps: a determination of the Flory-Huggins interaction parameters, followed by a conversion to DPD parameters. Here the Flory-Huggins interaction parameter (χ_{ij}) was calculated from the solubility parameters:

$$\chi_{ij} = (\delta_i - \delta_j)^2 v/RT \quad (3)$$

where R is the gas constant, T is the absolute temperature and v is the volume per mole beads. The DPD repulsion parameters a_{ij} can be related to the Flory-Huggins solubility parameter for density, in reduced units, of 3 as follows [34,35]:

$$a_{ij}\,(\rho = 3) = 25 + 3.5\chi_{ij} \quad (4)$$

where the a_{ij} are in reduced units.

The mass and volume of each bead is 108 amu and 180 Å^3, respectively, and the cutoff radius, r_c, between two beads is 8.14 Å. As illustrated in Figure 2, the p(NIPAM)$_{60}$-*b*-p(*L*-

DOPA)$_n$ polymer consists of 4 types of beads (A, B, C and F) and the Dox consists of 5 types beads (E1−E5), and the solubility parameter of each bead is derived by using Synthia or cohesive energy density calculations using Forcite Plus, COMPASS, and Amorphous Cell in Materials Studio 5.0 (Accelrys). The interaction parameters a_{ij} were calculated according to equation (4), as shown in Table 2. The diagonal elements used by Groot and Rabone are chosen such that a bead fluid has the compressibility of water [34]. A cubic simulation box with periodic boundary condition was applied in all directions. A box of 30 × 30 × 30 r_c^3 is enough to avoid the finite size effects, and the integration time step of 0.05 was small enough for our system to get thermodynamic equilibrium. The simulation steps of 200,000 were used. All simulations were carried out using the DPD method in Mesocite module of the commercial software package Materials Studio.

Table 2. Interaction Parameters a_{ij} between Different Beads in Figure 2(a)

	A	B	C	F	D1	D2	D3	D4	D5	W
A	25.00									
B	30.02	25.00								
C	31.09	38.15	25.00							
F	30.13	25.00	45.05	25.00						
D1	28.76	25.04	42.37	25.10	25.00					
D2	28.36	25.11	41.83	25.19	25.01	25.00				
D3	27.03	25.55	38.82	25.69	25.27	25.16	25.00			
D4	28.88	25.16	45.67	25.27	25.03	25.00	25.16	25.00		
D5	25.82	27.11	37.23	27.33	26.40	26.12	25.39	26.23	25.00	
W	168.20	238.11	34.90	222.76	212.57	212.35	200.10	250.38	212.36	25.00

All beads distributed randomly at the beginning of the simulation aggregate to form small clusters first and then turn into larger aggregates depending on the type and amount of polymer. As shown in Figure 2, p(NIPAM)$_{60}$-*b*-p(*L*-DOPA)$_{100}$ (P_{100}) beads tend to aggregate to form rod-like morphology at 10% aqueous solution and spherical nanocarriers at 5% aqueous solution. The self-assemblies of other polymers with different block lengths of *L*-DOPA also yield spherical nanocarriers. The hydrophobic beads of the polymer are distributed inside the nanocarrier forming a hydrophobic core and hydrophilic NIPAM and pyrocatechol beads spread around the surface, forming a protective shell.

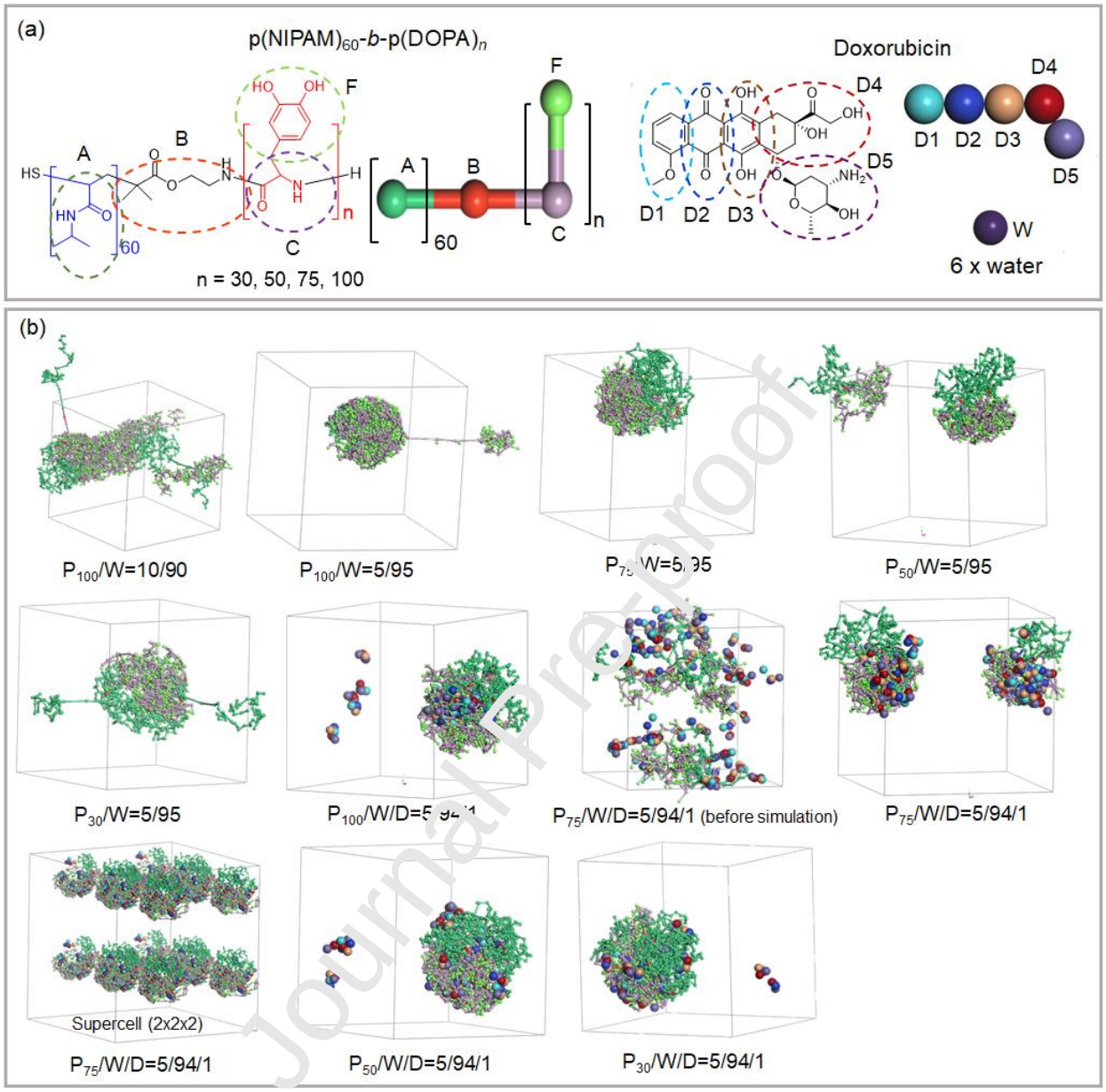

Figure 2. (a) Molecular structures and coarse-grained models of p(NIPAM)$_{60}$-*b*-p(*L*-DOPA)$_n$ (n = 30 (P_{30}), 50 (P_{50}), 75 (P_{75}), and 100 (P_{100})), doxorubicin (D), and water (W), and (b) configurations of polymer nanocarriers in the absence and presence of doxorubicin at different polymer P_n/W/D volume ratios. Doxorubicin beads are presented in CPK model, and water beads are not shown for clarity.

The similar morphological developments of the polymer beads are observed in the DPD simulations in the presence of 1% Dox. When the volume ratio of polymer:water:Dox is 5:89:1,

randomly distributed beads at the beginning of the simulation (Figure 2) aggregates to form spherical nanocarriers with stable structure with shell consisting of NIPAM and pyrocatechol fragments are formed at the early period of simulation less than 20,000 steps. Extra simulation steps to 200,000 gave no significant changes in the aggregate morphology. The Dox beads consisting of 5 different beads gradually diffuse into the nanocarriers and finally are distributed in the core of nanocarrier formed by the polymer beads, indicating that the nanocarrier formed by the dendrimer is a reasonable carrier for Dox. The block length of *L*-DOPA influences the efficiency of Dox encapsulation. When n is 35, 50, or 100 in p(NIPAM)$_{60}$-*b*-p(*L*-DOPA)$_n$, large portion of Dox remains free inside of simulation box without diffusing inside of polymer nanocarriers, while uniform spherical nanocarriers bearing Dox are formed at n=75 (see also (2x2x2) supercell). Comparing the self-assembly of p(NIPAM)$_{60}$-*b*-p(*L*-DOPA)$_{75}$ polymer in the absence and presence of Dox, one and two spherical nanocarriers are formed in a simulation box, respectively, which is in good agreement with experimental results. The nanocarrier size of the polymer formed in the absence of Dox is about 2-fold smaller than that of the nanocarriers fabricated in the presence of Dox.

3.3. Encapsulation of Dox and coordination of Fe^{3+}

For the encapsulation of Dox and the simultaneous formation of catechol-Fe^{3+} complex, micellization of p(NIPAM)$_{60}$-*b*-p(*L*-DOPA)$_{100}$ polymer in presence of Fe^{3+} ([DOPA]/[Fe^{3+}] = 2/1) and Dox. Similar to the self-assembly of pure polymers, the spherical nanocarriers were obtained with the average diameter of ~150 nm (Figure 1(b)) and the distribution of the nanocarriers remained unchanged without conspicuous broadening. The hydroxyl group of p(*L*-DOPA) could easily form the bis-catechol-Fe^{3+} complex at pH 7.4. Note that *L*-DOPA-based polypeptides possess fascinating chelating potential owing to the complex formation of catechol with Fe^{3+}. Interestingly, the equiliibrium constant for the reaction of bis and tris complexes formation possess high value in the range of 10^{40}–10^{45} [37]. Moreover, the bond between catechol and Fe^{3+} is remarkably strong that is closer to covalent bond binding energy [38]. Thus, the bis-catechol-Fe^{3+} complex may impart the resultant Dox-loaded nanocarriers stability in physiological conditions and especially in blood circulation, resulting in less toxicity to normal cells. The DLC and DLE of the nanocarriers were determined as 14.57% and 44.15% respectively. The Dox molecules were surrounded by the p(*L*-DOPA) block located in the core

of the nanocarriers, which might lead to improved Dox encapsulation capacity and efficiency via inter- and intra-molecular hydrophobic interactions.

3.4. Stimuli-responsive Dox release

Recently, Hwang and coworkers have showed that poly(ethylene glycol)-p(*L*-DOPA) polymer forms a stable bis-catechol–Fe^{3+} complex at pH 7.4 [24]. The complex in the drug-loaded p(*L*-DOPA) cores of the self-assembled micelles not only enhance micellar stability but also protect drug release efficiently in extracellular environments. Upon endocytosis, the bis-catechol–Fe^{3+} complex dissociated to the mono-complex in response to endosomal pH (pH 5.0) to trigger the facilitated intracellular drug release (see also Scheme 1). At different temperatures and pH condition, time-dependent release of Dox was evaluated using the Dox-loaded $p(NIPAM)_{60}$-$p(L\text{-DOPA})_{100}$–Fe^{3+} complex nanocarriers in phosphate buffered saline (PBS, pH 7.4). The drug release was evaluated by UV-Vis spectrometric monitoring at 480 nm, which is the characteristic absorption maximum of Dox in solution. The release performance was observed for 67 h with different temperatures and pH conditions, and the release profiles are shown in Figure 3. The transition temperature of p(NIPAM) significantly influenced the temperature-responsive release of Dox from the $p(NIPAM)_{60}$-$p(L\text{-DOPA})_{100}$ nanocarriers. Below LCST, p(NIPAM) chain is hydrophilic and forms the amphiphilic copolymer together with hydrophobic p(DOPA) and self-assembled to spherical nanocarriers having water soluble p(NIPAM) corona and water insoluble p(DOPA) core. Above LCST, the p(NIPAM) chain changes from hydrophilic to hydrophobic, consequently leading to low solubility and eventually to destabilize nanocarriers with leaking of payload from the destabilized nanocarriers. The Dox release results obtained at 25 °C, 37 °C and 42 °C confirm the influence of the p(NIPAM) block on the temperature-responsive release of Dox. The cumulative releases of Dox are estimated to be 18% and 25% at 25 °C and 37 °C, respectively. The Dox release is significantly enhanced when temperature is further increased to 42 °C, which is above the LCST of the polymer. The Dox release of about 35% is observed at 42 °C for 67 h.

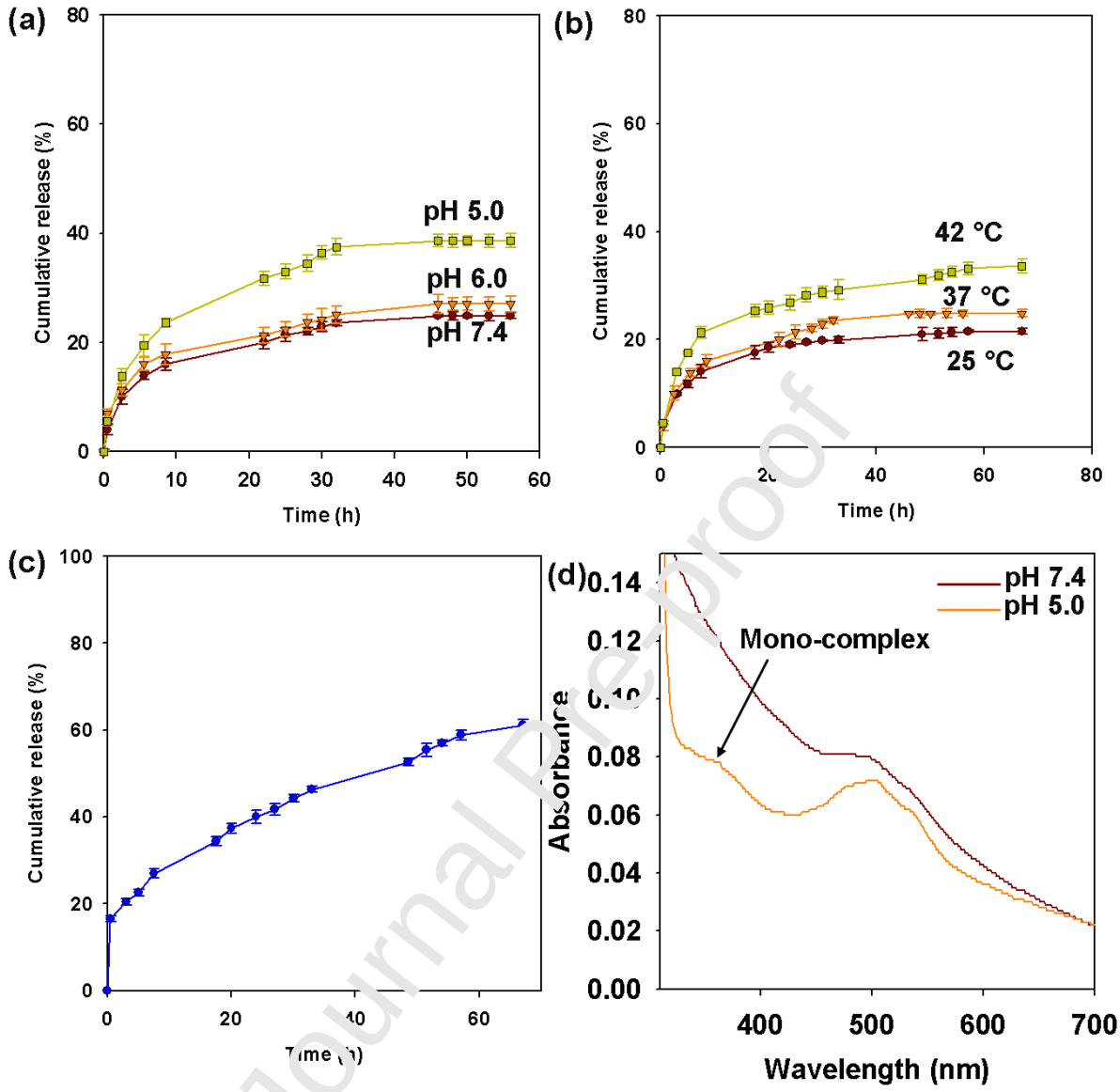

Figure 3. Time-dependent release of Dox from the nanocarriers fabricated by p(NIPAM)$_{60}$-*b*-p(DOPA)$_{100}$ conjugated with Fe^{3+} ions in phosphate-buffered saline (PBS) measured by (a) changing pH at 37 °C, (b) by changing temperature at pH 7.4, (c) at 42 °C and pH 5.0, and (d) UV-Vis absorption spectra of the Dox-loaded nanocarriers with catechol-Fe^{3+} complex at neutral and acidic conditions.

The time-dependent release of Dox from the nanocarrier was evaluated at different pH conditions to prove the pH-response of the polymer at 37 °C and at the temperature of cancer cells (42 °C). When the pH of the micellar solution decreased from 7.4 to 5.0, the cumulative release of Dox increased [Figure 3(a)] mainly due to the pH-responsive catechol–Fe^{3+} complex

in the nanocarrier, with transformation of the bis-complex to the mono-complex at pH 5.0 [Figure3(d)] [24]. Note that the bis-complex provides outstanding stability to nanocarriers, enhancing the retention of Dox at physiological conditions [24,39]. The Dox release from the nanocarriers bearing the catechol-Fe^{3+} complex was less than 20% at pH 7.4, whereas the Dox release from the nanocarriers fabricated in the absence of Fe^{3+} was more than 40% (Figure S11). These results clearly show that formation of the catechol-Fe^{3+} complex strongly inhibits the release of Dox by enhancing the stability of nanocarriers at pH 7.4. When pH decreased to 5.0, bis-complex to the mono-complex transformation destabilizes the nanocarrier and activates the simultaneous Dox release. At pH 5.0 and 42 °C, the Dox release reached 60% (Figure 3(c)). The results demonstrate that the catechol-Fe^{3+} complex contributes to stabilize nanocarriers in physiological conditions, which protects Dox from premature release, and that the rate and amount of Dox are tunable in response to temperature and pH mimicking the tumor cell conditions.

3.5. Cytotoxicity of p(NIPAM)$_{60}$-b-p(L-DOPA)$_n$

With an aim to demonstrate the biocompatibility of the p(NIPAM)$_{60}$-*b*-p(*L*-DOPA)$_n$, we have performed the cytotoxicity analysis. The effect of nanocarriers on cell viability was studied using both 293FT normal kidney cells and A2780 ovarian cancer cells lines with various concentrations of nanocarriers ranging from 0.1 to 100 μg/mL using the MTT assay. The viability of both the 293FT and A2780 cells lines are excellent (>90%) at all concentrations, irrespective of the increase in poly(*L*-DOPA) chain length (Figure 4). The diblock copolymers display low cytotoxicity in a wide nanocarrier concentration despite of the low biocompatibility of p(NIPAM) [40]. The p(DOPA) blocks may assist to achieve >90% cell viability by associating with the p(NIPAM) blocks by increasing the biocompatible component in the hydrophobic end. These results clearly illustrate that the nanocarriers formed from p(NIPAM)$_{60}$-*b*-p(*L*-DOPA)$_n$ have no acute and intrinsic cytotoxicity against both normal and cancer cells.

3.6. Cellular uptake and cytotoxicity of Dox-loaded p(NIPAM)$_{60}$-b-p(L-DOPA)$_{100}$ nanocarriers

To investigate the pH- and temperature-dependent antitumor effect of Dox-loaded polymer nanocarriers bearing catechol-Fe^{3+} complex against cancer cells, the Dox-loaded nanocarriers were incubated with A2780 for 24 h. Figure 5 shows that the cell viability exceeds 90% for all treatments including pH 5.6 at lower temperature (4 °C). While the viability decreases to 80% by

varying pH from 7.4 to 5.6 at 25 °C. The cell viability significantly decreases by changing 25 °C to 37 °C, in all pH conditions. It decreases monotonously by changing pH 7.4 to pH 6.8 and to pH 6.5. Finally, the cell viability reaches about 35% by decreasing pH 6.5 to pH 6.0 and to pH 5.6. These results prove that the rate and amount of Dox release are deeply associated with the temperature-responsive disassembly of the p(NIPAM) blocks and pH-responsive dissociation of catechol–Fe^{3+} complex in p(DOPA) blocks.

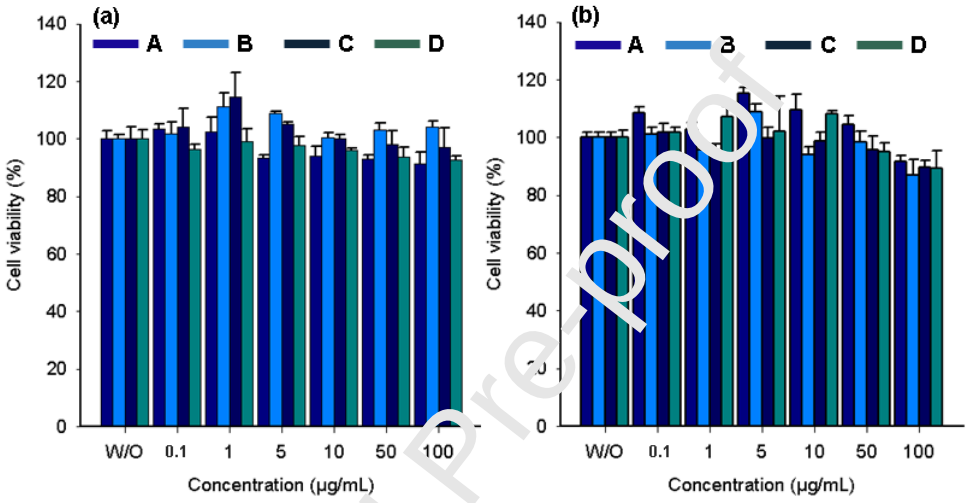

Figure 4. *In vitro* cell viability of p(NIPAM)$_{60}$-*b*-p(*L*-DOPA)$_n$ nanocarriers in (a) A2780 and (b) 293FT cells fabricated by (A) p(NIPAM)$_{60}$-*b*-p(*L*-DOPA)$_{30}$, (B) p(NIPAM)$_{60}$-*b*-p(*L*-DOPA)$_{50}$, (C) p(NIPAM)$_{60}$-*b*-p(*L*-DOPA)$_{75}$, and (D) p(NIPAM)$_{60}$-*b*-p(*L*-DOPA)$_{100}$.

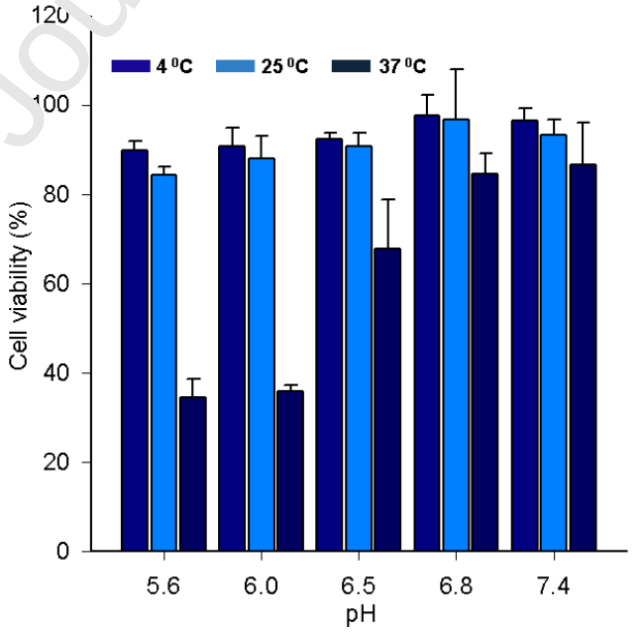

Figure 5. pH- and temperature-dependent cytotoxicity of Dox-loaded p(NIPAM)$_{60}$-*b*-p(*L*-DOPA)$_{100}$ nanocarriers bearing catechol–Fe^{3+} complex against A2780 cells after 24 h incubation.

The confocal laser scanning microscope (CSLM) images have been taken for the visualization of the pH- and temperature-dependent cellular uptake and Dox release from the Dox-loaded nanocarriers (Figure 6). The red fluourescence of Dox indicates the pH- and temperature-dependent Dox release in the tumor cells. The stronger fluorescence observed at pH 5.6 and 37 °C indicates the enhanced Dox release in the tumor environment. At low temperature (4 °C and 25 °C) and high pH (>6), no strong fluorescences are observed. The similar results are obseved at high pH and high temperature or at low pH and low temperature. Evidently the nanocarriers strongly hold the Dox in their catechol-Fe^{3+} complexed p(DOPA) hydrophobic core at non-cancerous environment and undergo destabilization and payload release under acidic pH and higher temperature, avoiding toxicity outside the tumor cells. The nanocarriers facilitate abundant Dox release in the tumor mimicking environment, resulting in remarkablly high fluorescent intensity at pH 5.6 and at 37 °C [Figure 6(c1)]. Additionally, Figure S12 displays the CSLM images of 293FT and A2780 cells incubated with 2 μM of nanocarriers for 24 h. The flow cytometry data (Figures S13 and S14) for the Dox-accumulated A2780 cells again confirm the temperature- and pH-responsive nature of nanocarriers. All of these results provide strong evidence for triggered Dox release into the cancer cells.

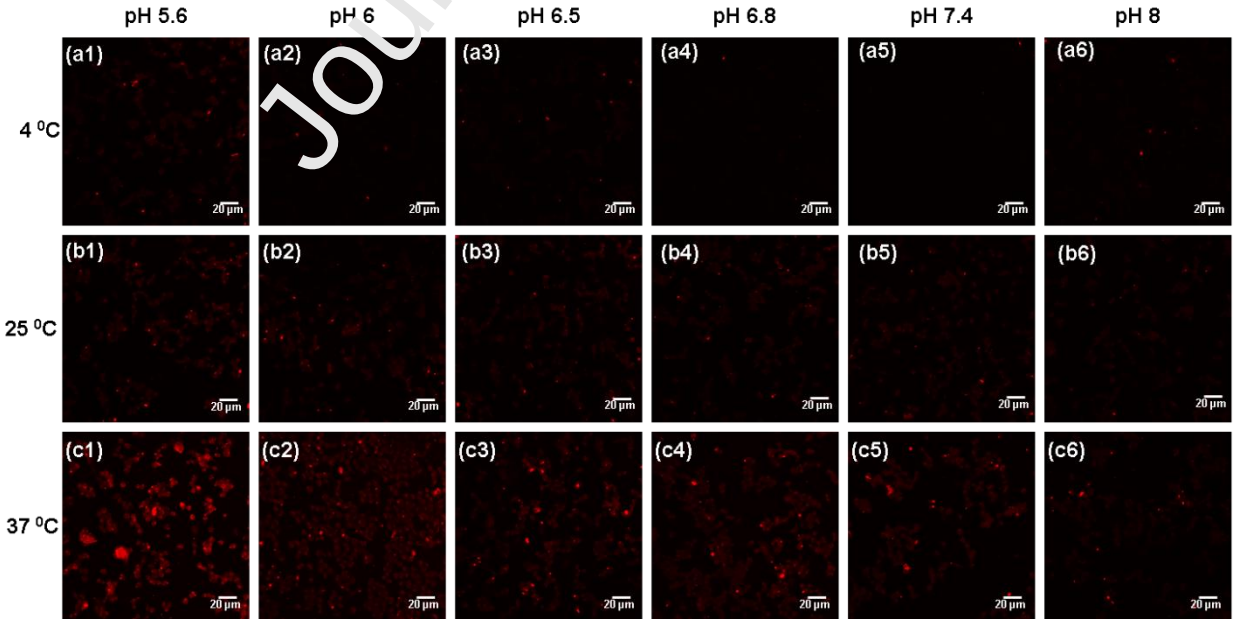

Figure 6. CSLM images of A2780 cells after 3 h incubation with 10 μM of Dox-loaded p(NIPAM)$_{60}$-*b*-p(*L*-DOPA)$_{100}$ nanocarriers, taken under different temperature and pH conditions.

3.7. In vivo bio-distribution

The Dox-loaded/ Fe^{3+}-complexed nanocarriers were injected into tumor-bearing mice, and after 72 h, the *in vivo* and *ex vivo* distributions were monitored using a Mastero 2 *in vivo* imaging system as illustrated in Figure 7. Remarkable Dox accumulation in the tumor cells was observed after 72 h from the *in vivo* (Figure 7C) and *ex vivo* (Figure 7F) fluorescence intensities compared to flluoresncence intensities from other organs. Especially the fluorescence intensities from organs such as heart, lung and spleen are negligible. Considering no specific active targeting groups are conjugated to the nanocarriers and no polymeric moieties or payloads that contribute to target to specific cells are involved, the nanocarriers of this study are expected to possess no specific targetability to tumor cells. Unexpectedly, the nanocarriers showed considerable Dox accumulation in the tumor cells after 72 h via an EPR effect, offering an effective passive targetability to cancer cells [41].

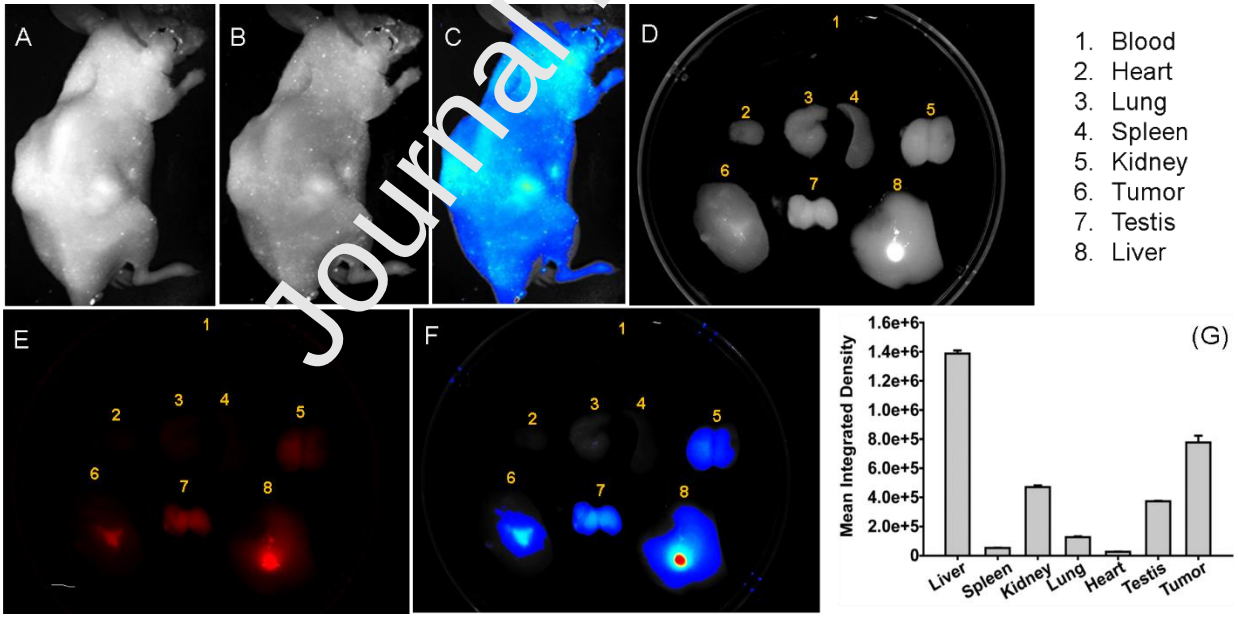

Figure 7. Representative white light and RFP fluorescence images of (A−C) mouse and (D−H) major organs and tumor taken 72 h after administration and (G) quantitative analysis of fluorescence intensity from each organ.

Ex vivo measurements were conducted by sacrificing the mice 72 h after injecting the Dox-loaded nanocarriers. Fluorescence analysis was conducted and quatntitatively calculated the intensity from each organs by collecting major organs. The *ex vivo* fluorescence intensities from the different organs are shown in Figures 7E–F and their quatntitatively calculated intensity is summarized in Figure 7G. The fluorescence intensity was remarkably higher in the tumor tissues than in other organs such as blood, heart, lung and spleen, which is well match with the *in vivo* biodistribution image and validates the effective tumor internalization. The quantitative intensity analysis confirms the results. The intensity in tumor is higher than in kidney by almost 2-fold. The intensity from blood, heart, lungs and spleen is almost zero or closed to zero, which implys less toxicity to normmal cells. The high intensity in the liver tissues is due to the intrinsic absorption of the tissues and their light scattering capacity [42,43].

4. Conclusions

A series of dual-stimuli-responsive block copolymers, p(NIPAM)$_{60}$-*b*-p(*L*-DOPA)$_n$ (n = 30, 50, 75, 100) were sucessfully synthesized using the RAFT polymerization, followed by the ROP of DOPA-NCA using the p(NIPAM)$_{60}$–NH_2 as a macroinitiator in the presence of the ICy·HCO_3 organocatalyst. Spherical nanoparticle of ~100 nm was fabricated by the self-assembly. The similar self-assembly of p(NIPAM)$_{60}$-*b*-p(*L*-DOPA)$_n$ in the presence of Dox and Fe^{3+} ions that induce catechol-Fe^{3+} complex led to form highly uniform and robust nanocarriers of ~150 nm with effective DLC (14.57%) and DLE (44.15%). The resultant nanocarriers showed favorable pH- and temperature-responsive Dox release behaviors. The pH- and temperature-responsive cellular uptakes of the nanocarriers resulting in enhanced antitumor activity were also demonstrated with the A2780 ovarian cancer cells. The significant tumor accumulation was also confirmed via *in vivo* and *ex vivo* biodistribution analyses. The dual-stimuli-responsive nanocarriers fabricated by p(NIPAM)$_{60}$-*b*-p(*L*-DOPA)$_n$ copolymers conjugated with Fe^{3+} ions showing the successful passive targeting capability based on EPR effect are considered to be a promising platform for theranostic application.

Conflicts of interest

There are no conflicts to declare.

Data availability statement

The raw/processed data required to reproduce these findings cannot be shared at this time as the data also forms part of an ongoing study.

Acknowledgements

This research was supported by the Basic Science Research Program through the National Research Foundation of Korea (2018R1D1A1A09081809) and Korea Health Technology R&D Project, Ministry of Health and Welfare (HI17C1635). The authors thank Korea Basic Science Institute for providing the partial financial support.

References

[1] I. Gashaw, P. Ellinghaus, A. Sommer, K. Asadullah, What makes a good drug target?, Drug Discov. Today 16 (2011)1037–1043.

[2] S. Yu, D. Zhang, C. He, W. Sun, R. Xiao, S. Cui, M. Deng, Z. Gu, X. Chen, Injectable thermosensitive polypeptide-based CL/DP-complexed hydrogel for improving localized antitumor efficacy, Biomacromolecules 18 (2017) 4341–4348.

[3] R.-M. Jin, M.-H. Yao, J. Yang, D.-H. Zhao, Y.-D. Zhao, B. Liu, One-step in situ synthesis of polypeptide–gold manoparticles hybrid nanogels and their application in targeted photoacoustic imaging, ACS Sustain. Chem. Eng. 5 (2017) 9841–9847.

[4] C. Ge, L. Zhao, Y. Ling, H. Tang, Thermo and pH dual responsive polypeptides derived from "clickable" poly([gamma]-3-methylthiopropyl-l-glutamate), Polym. Chem. 8 (2017) 1895–1905.

[5] R.P. Johnson, S. Uthaman, R. Augustine, Y. Zhang, H. Jin, C.I. Choi, I.-K. Park, I. Kim, Glutathione and endosomal pH-responsive hybrid vesicles fabricated by zwitterionic polymer block poly(l-aspartic acid) as a smart anticancer delivery platform, React. Funct. Polym. 119 (2017) 47–56.

[6] J.V. John, S. Uthaman, R. Augustine, K. Manickavasagam Lekshmi, I.-K. Park, I. Kim, Biomimetic pH/redox dual stimuli-responsive zwitterionic polymer block poly(L-histidine)

micelles for intracellular delivery of doxorubicin into tumor cells, J. Polym. Sci. Polym. Chem. 55 (2017) 2061–2070.

[7] T.-M. Don, K.-Y. Lu, L.-J. Lin, C.-H. Hsu, J.-Y. Wu, F.-L. Mi, Temperature/pH/enzyme triple-responsive cationic protein/PAA-b-PNIPAAm nanogels for controlled anticancer drug and photosensitizer delivery against multidrug resistant breast cancer cells, Mol. Pharm. 14 (2017) 4648–4660.

[8] N.A. Estrich, A. Hernandez-Garcia, R. de Vries, T.H. LaBean, Engineered diblock polypeptides improve DNA and gold solubility during molecular assembly, ACS Nano 11 (2017) 831–842.

[9] E. Garanger, S.R. MacEwan, O. Sandre, A. Brûlet, L. Bataille, A. Chilkoti, S. Lecommandoux, Structural evolution of a stimulus-responsive diblock polypeptide micelle by temperature tunable compaction of its core, Macromolecules 48 (2015) 6617–6627.

[10] M.A. Quadir, S.W. Morton, Z.J. Deng, K.E. Shopsowitz, R.P. Murphy, T.H. Epps, P.T. Hammond, PEG–polypeptide block copolymers as pH-responsive endosome-solubilizing drug nanocarriers, Mol. Pharm. 11 (2014) 2420–2430.

[11] Z. Cao, H. Wu, J. Dong, G. Wang, Quadruple-stimuli-sensitive polymeric nanocarriers for controlled release under combined stimulation, Macromolecules 47 (2014) 8777–8783.

[12] Y. Chen, X. Li, H. Xiao, J. Xiao, B. Li, X. Chen, Y. Wang, D. Cheng, X. Shuai, Reduction and pH dual-sensitive nanovesicles co-delivering doxorubicin and gefitinib for effective tumor therapy, RSC Adv. 8 (2018) 2082–2091.

[13] F. Karandish, J. Froberg, P. Borowicz, J.C. Wilkinson, Y. Choi, S. Mallik, Peptide-targeted, stimuli-responsive polymersomes for delivering a cancer stemness inhibitor to cancer stem cell microtumors, Colloids surface. B 163 (2017) 225–235.

[14] H. He, R. Zhu, W. Sun, K. Cai, Y. Chen, L. Yin, Selective cancer treatment via cascaded photodynamic sensitization of hypoxia-responsive drug delivery, Nanoscale 10 (2017) 2856–2865.

[15] Y. Ma, X. Wang, H. Chen, Z. Miao, G. He, J. Zhou, Z. Zha, Polyacrylic acid functionalized $Co_{0.85}Se$ nanoparticles: an ultrasmall pH-responsive nanocarrier for synergistic photothermal-chemo treatment of cancer, ACS Biomater. Sci. Eng. 4 (2017) 547–557.

[16] V. Chrysostomou, S. Pispas, Stimuli-responsive amphiphilic PDMAEMA-b-PLMA copolymers and their cationic and zwitterionic analogs, J. Polym. Sci. Polym. Chem. 56 (2018) 598–610.

[17] W. Lin, Q. Hu, K. Jiang, Y. Cui, Y. Yang, G. Qian, A porous Zn-based metal-organic framework for pH and temperature dual-responsive controlled drug release, Micropor. Mesopor. Mater. 249 (2017) 55–60.

[18] X. Peng, P. Liu, B. Pang, Y. Yao, J. Wang, K. Zhang, Facile fabrication of pH-responsive nanoparticles from cellulose derivatives via Schiff base formation for controlled release, Carbohydrate Polymers 216 (2019) 113–118.

[19] F. Liu, V. Kozlovskaya, S. Medipelli, B. Xue, F. Ahmad, M. Saeed, D. Cropek, E. Kharlampieva, Temperature-sensitive polymersomes for controlled delivery of anticancer drugs, Chem. Mater. 27 (2015) 7945–7956.

[20] P.F. Gao, L.L. Zheng, L.J. Liang, X.X. Yang, Y.F. Li, C.Z. Huang, A new type of pH-responsive coordination polymer sphere as a vehicle for targeted anticancer drug delivery and sustained release, J. Mater. Chem. B 1 (2013) 3202–3208.

[21] T. Wang, D. Wang, H. Yu, M. Wang, J. Liu, B. Feng, F. Zhou, Q. Yin, Z. Zhang, Y. Huang, Y. Li, Intracellularly acid-switchable multifunctional micelles for combinational photo/chemotherapy of the drug-resistant tumor, ACS Nano 10 (2016) 3496–3508.

[22] X. Wang, Y. Yang, Y. Zhuang, P. Gao, F. Yang, H. Shen, H. Guo, D. Wu, Fabrication of pH-responsive nanoparticles with an AIE feature for imaging intracellular drug delivery, Biomacromolecules 17 (2016) 2920–2929.

[23] J.H. Waite, N.H. Andersen, S. Jewhurst, C. Sun, Mussel adhesion: finding the tricks worth mimicking, J. Adhesion 81 (2005) 297–317.

[24] G.H. Hwang, K.H. Min, H.J. Lee, H.Y. Nam, G.H. Choi, B.J. Kim, S.Y. Jeong, S.C. Lee, pH-Responsive robust polymer micelles with metal-ligand coordinated core cross-links, Chem. Commun. 50 (2014) 4351–4353.

[25] S.M. Janib, A.S. Moses, J.A. MacKay, Imaging and drug delivery using theranostic nanoparticles, Adv. Drug Deliv. Rev. 62 (2010) 1052–1063.

[26] R.P. Johnson, Y.I. Jeong, J.V. John, C.-W. Chung, D.H. Kang, M. Selvaraj, H. Suh, I. Kim, Dual stimuli-responsive Poly(N-isopropylacrylamide)-b-poly(l-histidine) chimeric materials for

the controlled delivery of doxorubicin into liver carcinoma, Biomacromolecules 14 (2013) 1434–1443.

[27] M.S.V. W. D. Fuller, M. Goodman, , DOPA-containing polypeptides. I. Improved synthesis of high-molecular-weight poly(L-DOPA) and water-soluble copolypeptides, Biopolymers 17 (1978) 2939.

[28] Y. Zhang, R. Liu, H. Jin, W. Song, R. Augustine, I. Kim, Straightforward access to linear and cyclic polypeptides, Commun Chem (2018) 1(1) 40.

[29] J.V. John, C.-W. Chung, R.P. Johnson, Y.-I. Jeong, K.-D. Chung, D.H. Kang, H. Suh, H. Chen, I. Kim, Dual stimuli-responsive vesicular nanospheres fabricated by lipopolymer hybrids for tumor-targeted photodynamic therapy, Biomacromolecules 17 (2016) 20–31.

[30] G. Moad, RAFT polymerization to form stimuli-responsive polymers, Polym. Chem. 8 (2017) 177–219.

[31] R. Augustine, D.-K. Kim, J.V. John, J.H. Kim, I. Kim, Dual-stimuli responsive amphiphilic chimeric triblock copolymer hybrid micelles for anticancer drug delivery, J. Control. Release 259 (2017) e116–e117.

[32] Y. Lv, Q. Pan, S.W.A. Bligh, H. Li, H. Wu, Q. Sang, L.-M. Zhu, Core-sheath nanofibers as drug delivery system for thermoresponsive controlled release, J. Pharm. Sci. 106 (2017) 1258–1265.

[33] P.J. Hoogerbrugge, J.M.V.A. Koelman, Simulating microscopic hydrodynamic phenomena with dissipative particle dynamics, EPL Europhys. Lett. 19 (1992) 155–160.

[34] P. Español, P. Warren, Statistical mechanics of dissipative particle dynamics, EPL Europhys. Lett. 30(4) (1995) 191–196.

[35] R.D. Groot, K.L. Rabone, Mesoscopic simulation of cell membrane damage, morphology change and rupture by nonionic surfactants, Biophys. J. 81 (2001) 725–736.

[36] R.D. Groot, P.B. Warren, Dissipative particle dynamics: Bridging the gap between atomistic and mesoscopic simulation, J. Chem. Phys. 107 (1997) 4423–4435.

[37] A. Avdeef, S.R. Sofen, T.L. Bregante, K.N. Raymond, Coordination chemistry of microbial iron transport compounds. 9. Stability constants for catechol models of enterobactin, J. Am. Chem. Soc. 100 (1978) 5362–5370.

[38] H. Lee, N.F. Scherer, P.B. Messersmith, Single-molecule mechanics of mussel adhesion, Proc. Natl. Acad. Sci. USA 103 (2006) 12999–13003..

[39] H.Y. Nam, K.H. Min, D.E. Kim, J.R. Choi, H.J. Lee, S.C. Lee, Mussel-inspired poly(L-DOPA)-templated mineralization for calcium phosphate-assembled intracellular nanocarriers, Colloid. Surface. B 157 (2017) 215–222.

[40] M.A. Cooperstein, H.E. Canavan, Assessment of cytotoxicity of (N-isopropyl acrylamide) and poly(N-isopropyl acrylamide)-coated surfaces, Biointerphases 8 (2013) 19.

[41] J.V. John, E.J. Seo, R. Augustine, I.H. Jang, D.K. Kim, Y.W. Kwon, J.H. Kim, I. Kim, Phospholipid end-capped bioreducible polyurea micelles as a potential platform for intracellular drug delivery of doxorubicin in tumor cells, ACS Biomater. Sci. Eng. 2 (2016) 1883–1893.

[42] X. Cai, D. Mao, C. Wang, D. Kong, X. Cheng, B. Liu, Multifunctional liposome: A bright AIEgen–lipid conjugate with strong photosensitization, Angew. Chem. Int. Ed. Engl. 57 (2018) 16396–16400.

[43] H. Jin, T. Zhu, X. Huang, M. Sun, H. Li, X. Zhu, M. Liu, Y. Xie, W. Huang, D. Yan, ROS-responsive nanoparticles based on amphiphilic hyperbranched polyphosphoester for drug delivery: Light-triggered size-reducing and enhanced tumor penetration, Biomaterials 211 (2019) 68–80.

CREDIT AUTHOR STATEMENT

Rimesh Augustine: Conceptualization; Methodology; Data curation; Investigation; Writing-Original draft; Writing-review and Editing.

Dae-Kyoung Kim: Conceptualization; Methodology; Data curation; Investigation; Writing-Original draft.

Su Hyeon Jeon: Methodology; Data curation; Validation.

Tae Wook Lee: Methodology; Data curation; Validation.

Nagendra Kalva: Conceptualization; Writing-Reviewing and Editing.

Jae Ho Kim: Resources; Supervision; Project administration; Funding acquisition.

Il Kim: Resources; Supervision; Writing-Original draft; Writing-Reviewing and editing; Project administration; Funding acquisition.

Declaration of interests

☒ The authors declare that they have no known competing financial interests or personal relationships that could have appeared to influence the work reported in this paper.

☐The authors declare the following financial interests/personal relationships which may be considered as potential competing interests:

Graphical abstracts:

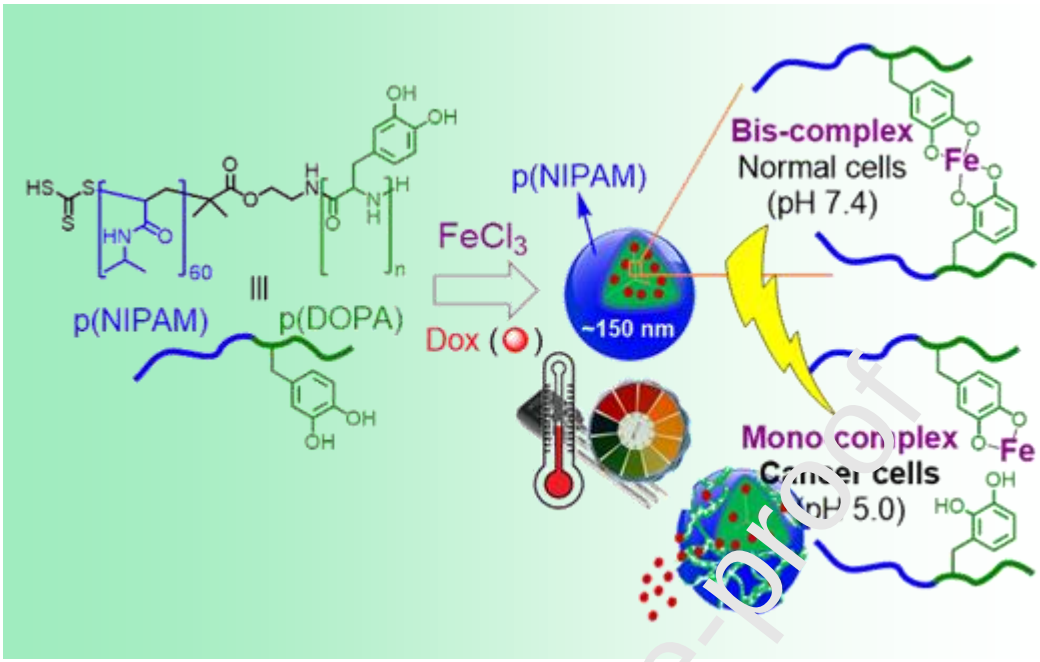

Highlights:

- Dual-stimuli-responsive polymers are synthesized by combining RAFT with ROP.
- The Fe^{3+} conjugated nanocarriers display remarkable T/pH-responsive Dox release.
- The Dox-loaded nanocarriers show intense cell uptake & cytotoxicity to cancer cells.
- The nanocarriers exhibit a remarkable tumor accumulation by EPR effect.